Nonlinear Control of Hybrid Drones via Optimised Control Allocation

Gil Silvestre Serrano
gil.serrano@tecnico.ulisboa.pt

Instituto Superior Técnico, Lisboa, Portugal

January 2021

Abstract

This dissertation addresses the development of a unified control strategy, based on nonlinear control techniques, for hybrid UAVs, more precisely tri-tiltrotor UAVs, so that a simple trajectory is followed. First, the model of a tri-tiltrotor UAV is derived, detailing the forces and moments that act on the system. Then, a unified control approach that considers the system dynamics as a whole is developed. To this effect, backstepping control and nonlinear optimisation are used for position and attitude control to calculate force and moment references. To allocate these references, a control allocation strategy based on nonlinear optimisation is proposed. Next, two trajectories characterised by an upward motion segment and a forward motion segment, each with a different forward velocity value, are defined. In the first trajectory, the UAV is expected to fully transition from rotary-wing to fixed-wing configuration, while in the second trajectory, the objective is to have the UAV fly in an intermediate configuration. To validate the control approach, simulations for the defined trajectories are performed and the results are analysed. Finally, the instrumentation of a tiltrotor UAV is described and verified with a test flight.

Keywords: Hybrid UAV, Tiltrotor UAV, Backstepping control, Control Allocation, Trajectory tracking

1. Introduction

The usage of UAVs has grown considerably over the past years as more applications, whether military, civilian or in academia, are found for these vehicles. Depending on the nature of the application, the type of UAV that has the best performance for a certain task may vary. Fixed-wing and rotary-wing UAVs are ubiquitous. Despite their predominance, both types of UAV are not without flaw. Each presents a distinct set of advantages and disadvantages. A different type of UAV attempts to mitigate the shortcomings and combine the strengths of both fixed-wing and rotary-wing aircraft - hybrid UAVs. These UAVs are typically fixed-wing vehicles with VTOL capabilities, which enables them to be more effective in a wider range of application scenarios. However, hybrid UAVs are complex vehicles and therefore pose additional challenges in modelling and control.

1.1. Motivation

The motivation for this work stems from the opportunity to take advantage of the characteristics of hybrid UAVs in applications in which fixed and rotary-wing UAVs do not perform as adequately. Hybrid aircraft combine features of fixed-wing and rotary-wing aircraft in order to take advantage of the best performance aspects of both types of UAVs and lessen the drawbacks. The ability to fly at high speeds, with a long flight range and greater payload capacity, coupled with the possibility to vertically take off and land without a runway, give hybrid UAVs more manoeuvrability and a wider range of application scenarios than fixed-wing or rotary-wing UAVs. The operation of these aircraft is usually divided into three modes: hover, transition, and cruise flight.

This work was developed within the scope of the REPLACE project [1], which intends to develop a package delivery system in urban environments using UAVs. This project addresses the problem of vehicle autonomy and flight distance by exchanging parcels between UAVs, thus extending the possible delivery range. This presents a plethora of challenges in, for example, cooperative control of a heterogeneous UAV system, path planning, trajectory tracking, and logistics. Hybrid UAVs offer some features, such as improved range and the ability to vertically take off in a confined environment, which would be beneficial for such a delivery system.

1.2. Objectives

This work addresses the design of nonlinear control techniques for trajectory tracking with hybrid UAVs, more precisely, tiltrotor UAVs.

The usual control approach for hybrid vehicles is to employ hybrid control techniques, defining several modes of working that are less complex than the entire system, developing controllers for each mode, and switching between them as required to control the vehicle. In the case of hybrid UAV, a common approach is to consider a rotary-wing or multicopter mode and a fixed-wing mode for this type of vehicles. One of the objectives of this work is to take the initial steps towards a unified control approach to tiltrotor UAVs, considering the system as a whole, instead of having different modes of operation, as will be seen. By not dividing the system into different modes, another goal is to have the UAV fly in an intermediate configuration, neither fully in rotary-wing nor in fixed-wing mode. To achieve this, a trajectory that takes the aircraft up to a certain altitude and then begins flying forward will be devised. Next, taking into account a dynamic model of the UAV, the unified nonlinear control strategy will be derived and tested in simulation to check if the vehicle behaves as intended and flies in an intermediate configuration.

1.3. Outline

The remainder of this work is organised as follows. Section 2 provides a brief overview of research on hybrid UAVs. Section 3 describes the nonlinear model of a tri-tilrotor UAV. Section 4 delineates the unified control approach, using backstepping to control the position and attitude of the UAV, as well as the control allocation scheme, based on nonlinear optimisation. Section 5 describes the reference trajectories and presents the simulation results and the evaluation of the performance. Section 6 describes the instrumentation of a tiltrotor UAV. Finally, Section 7 summarises the work developed and assesses what is still to be done as future work.

2. Related Work

The past decade has seen an increase in research work on hybrid UAV. Much work is focused on developing control algorithms that target one of the operation modes of these vehicles, while others opt for a more comprehensive approach to the problem. Control methods for hybrid UAV usually employ hybrid control techniques, which consist of designing controllers for each operation mode and switching between them, while guaranteeing that the system remains stable during the transition.

Regarding hybrid control of tri-tiltrotor UAVs, in [2], the dynamical model of the aircraft is divided into two situations: in hover mode, in which aerodynamic effects are neglected, and in cruise flight mode, with a simplified model of these effects. The control strategy takes into account the longitudinal dynamics for altitude and attitude control, i.e. only pitch motion is stabilised by a PID controller, with roll and yaw controlled manually. The defined trajectory has a trapezoidal velocity profile, meaning that the aircraft accelerates at a constant value until a certain velocity is reached, maintaining that velocity until it start decelerating also at a constant value. The modelling and control of a tri-tiltrotor UAV is also the subject of [3], though only for hover mode. An attitude PID controller and a control allocation scheme based on the desired roll and pitch moments and (vertical) thrust are designed, tested in simulation and experimentally with adequate results in altitude stability, despite a more oscillatory behaviour in terms of attitude control. A more complete nonlinear model of a tri-tiltrotor UAV is derived in [4], with emphasis on transition dynamics, studied in computational fluid dynamics simulation. A hybrid approach that switches between hover, transition and cruise flight controllers is implemented and simulation results show that the UAV is not able to maintain the altitude, which decreases with every controller switch.

Unified approaches to control of hybrid UAV, though less common than hybrid approaches, have also been developed. In [5], the flight envelope of a tiltwing UAV is studied and modelled via wind tunnel tests, defining a continuous flight configuration space that contains the different flight modes, thus not needing to define discrete flight configurations. With this strategy, a map-based feedforward controller independent of the flight state for motion control is developed. The tilt angle of the wing is obtained in conjunction with the aircraft's pitch angle dependent on the flight state. The approach in [6], for a quad-tailsitter UAV, handles the flight modes in a continuous fashion as well. Unlike the previous example, in the case of a tailsitter, the aircraft's attitude changes significantly across the flight envelope, as there is no tilting mechanism to change the direction of the thrust generated by the rotors. To deal with this, the controller solves a nonlinear optimisation problem to compute the required attitude and thrust. In July 2020, Auterion announced that they are developing a novel approach to control allocation based on dynamic computation of input effectiveness matrices [7], that was shown to allow a single form of control allocation for hybrid UAV, instead of different control allocation schemes for each flight mode. The performance was demonstrated with an *E-Flite Convergence VTOL*, represented in Figure 1, which was able to fly in an intermediate configuration. There are still many limitations with this approach for hybrid UAV, since the effectiveness matrix calcu-

lation is done by linearising the input influence on the dynamics around a constant trim point. As such, the UAV cannot fly in cruise flight and there are constraints on the tilt angles due to the linearisation not being valid in every flight configuration. Nonetheless, it is a considerable step towards a unified control structure for tiltrotor UAV.

3. Modelling

This section presents the modelling concepts used in this work. The model is based on the *E-Flite Convergence VTOL*.

3.1. Coordinate Frames

To define the rigid-body kinematics, it is first necessary to define an inertial frame of reference $\{\mathcal{I}\} = \{O_\mathcal{I};\ \hat{\boldsymbol{\imath}}_\mathcal{I},\ \hat{\boldsymbol{\jmath}}_\mathcal{I},\ \hat{\boldsymbol{k}}_\mathcal{I}\}$, which will be a local NED frame [8], and a body frame $\{\mathcal{B}\} = \{O_\mathcal{B};\ \hat{\boldsymbol{\imath}}_\mathcal{B},\ \hat{\boldsymbol{\jmath}}_\mathcal{B},\ \hat{\boldsymbol{k}}_\mathcal{B}\}$. The origin $\{\mathcal{I}\}$ is a fixed point on the earth's surface $O_\mathcal{I}$, the x-axis $\hat{\boldsymbol{\imath}}_\mathcal{I}$ points north, the y-axis $\hat{\boldsymbol{\jmath}}_\mathcal{I}$ points east, and the z-axis $\hat{\boldsymbol{k}}_\mathcal{I}$ points towards the earth in the direction of the plane's normal. Frame $\{\mathcal{B}\}$ is defined by having its origin $O_\mathcal{B}$ on the UAV's centre of mass (CoM), the x-axis $\hat{\boldsymbol{\imath}}_\mathcal{B}$ pointing forward, the y-axis $\hat{\boldsymbol{\jmath}}_\mathcal{B}$ pointing to the right, and the z-axis $\hat{\boldsymbol{k}}_\mathcal{B}$ pointing downward.

The UAV has two tilting rotors that tilt longitudinally in a pitching motion. Following the approach in [9], two more coordinate frames $\{\mathcal{T}_1\}$ and $\{\mathcal{T}_2\}$ are introduced, one for each tilting rotor. Assigning $\{\mathcal{T}_1\} = \{O_{\mathcal{T}_1};\ \hat{\boldsymbol{\imath}}_{\mathcal{T}_1},\ \hat{\boldsymbol{\jmath}}_{\mathcal{T}_1},\ \hat{\boldsymbol{k}}_{\mathcal{T}_1}\}$to the right rotor, with x-axis $\hat{\boldsymbol{\imath}}_{\mathcal{T}_1}$ aligned along the spin axis, pointing forward, y-axis $\hat{\boldsymbol{\jmath}}_{\mathcal{T}_1}$ aligned with the tilting axis, pointing right, and z-axis $\hat{\boldsymbol{k}}_{\mathcal{T}_1}$ pointing downward (when the rotor is tilted forward). The origin $O_{\mathcal{T}_1}$ is thus defined as the point where the generated force is applied. The coordinate frame $\{\mathcal{T}_2\}$ for the left rotor is defined similarly. The positions of the origins of $\{\mathcal{T}_1\}$ and $\{\mathcal{T}_2\}$, with respect to $\{\mathcal{B}\}$, are $\mathbf{r}_1 = \begin{bmatrix} r_{1,x} & r_{1,y} & r_{1,z}\end{bmatrix}^\mathsf{T}$ and $\mathbf{r}_2 = \begin{bmatrix} r_{2,x} & r_{2,y} & r_{2,z}\end{bmatrix}^\mathsf{T}$, respectively. Let γ_1 and γ_2 denote the right and left rotors' tilt angles, respectively. Considering $i = \{1, 2\}$, the orientation of $\{\mathcal{T}_i\}$ relative to $\{\mathcal{B}\}$ is given by the rotation matrix

$$
{}^\mathcal{B}_{\mathcal{T}_i}\mathbf{R}(\gamma_i) = \begin{bmatrix} \cos(\gamma_i) & 0 & \sin(\gamma_i) \\ 0 & 1 & 0 \\ -\sin(\gamma_i) & 0 & \cos(\gamma_i) \end{bmatrix} \tag{1}
$$

These frames are represented graphically in Figure 1.

3.2. Aerodynamic Forces and Moments

Aerodynamic phenomena are significant for hybrid UAVs. The aerodynamic forces, $\mathbf{F}_\text{aero}$, and moments, $\mathbf{M}_\text{aero}$, are divided into two categories: longitudinal and lateral. The model follows [8], with some adaptations.

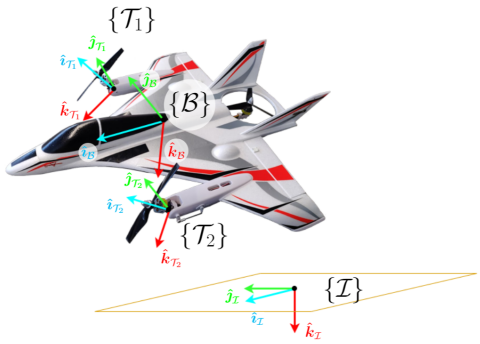

Fig. 1: Coordinate frames

3.2.1 Longitudinal Aerodynamics

We start by considering the lift force, $\mathbf{F}_\text{Lift}$, and drag force, $\mathbf{F}_\text{Drag}$, with magnitudes given by

$$
\begin{aligned}
F_\text{Lift} &= \frac{1}{2}\rho S(C_\text{L}(\alpha) + (1-\sigma(\alpha))C_{\text{L},\delta_\text{e}}\delta_\text{e})\|{}^\mathcal{B}\mathbf{v}\|^2, \\
F_\text{Drag} &= \frac{1}{2}\rho S(C_\text{D}(\alpha) + (1-\sigma(\alpha))C_{\text{D},\delta_\text{e}}\delta_\text{e})\|{}^\mathcal{B}\mathbf{v}\|^2,
\end{aligned} \tag{2}
$$

with air density ρ, wing surface area S, body velocity ${}^\mathcal{B}\mathbf{v} = \begin{bmatrix} u & v & w\end{bmatrix}^\mathsf{T}$, lift and drag coefficients $C_\text{L}(\alpha)$ and $C_\text{D}(\alpha)$, angle of attack $\alpha = \text{atan2}(w, u)$, lift and drag coefficients $C_{\text{L},\delta_\text{e}}$ and $C_{\text{D},\delta_\text{e}}$ related to the elevator angle δ_e. Function $\sigma(\alpha)$ is a sigmoid function of the angle of attack. The elevator angle δ_e is given by $\delta_\text{e} = \delta_{\text{e,r}} + \delta_{\text{e,l}}$, with $\delta_{\text{e,r}}$ and $\delta_{\text{e,l}}$ the right and left elevon angles. The lift and drag coefficients are given by

$$
\begin{aligned}
C_\text{L}(\alpha) &= (1-\sigma(\alpha))\,(C_{\text{L},0} + C_{\text{L},\alpha}\,\alpha) + \\
&\quad \sigma(\alpha)\,(2\,\text{sign}(\alpha)\,\sin^2(\alpha)\,\cos(\alpha))\,, \\
C_\text{D}(\alpha) &= C_\text{parasitic} + \frac{(C_{\text{L},0} + C_{\text{L},\alpha}\,\alpha)^2}{(\pi\, e_\text{Osw}\ AR)}\,,
\end{aligned} \tag{3}
$$

with $C_{\text{L},0}$ being the value of the lift coefficient when $\alpha = 0$, $C_{\text{L},\alpha}$ the coefficient of a linear term, $C_\text{parasitic}$ a coefficient related to parasitic drag, e_Osw the Oswald efficiency factor, and AR the UAV aspect ratio. The function $\sigma(\alpha)$ is a sigmoid function given by

$$
\sigma(\alpha) = \frac{1 + e^{-M(\alpha-\alpha_0)} + e^{M(\alpha-\alpha_0)}}{(1+e^{-M(\alpha-\alpha_0)})\,(1+e^{M(\alpha-\alpha_0)})} \tag{4}
$$

with M and α_0 positive constants. It is mostly used as a weight, so as to give more importance to aerodynamic phenomena when the angle of attack is smaller than a certain angle α_0, and less importance otherwise, since when the UAV functions in rotary-wing mode, aerodynamics do not have as great an influence as in fixed-wing mode.

The longitudinal aerodynamic force components $F_{\text{aero},i}$ and $F_{\text{aero},k}$ are given by

$$
\begin{bmatrix} F_{\text{aero},i} \\ F_{\text{aero},k} \end{bmatrix} = \begin{bmatrix} \cos(\alpha) & -\sin(\alpha) \\ \sin(\alpha) & \cos(\alpha) \end{bmatrix} \begin{bmatrix} -F_\text{Drag} \\ -F_\text{Lift} \end{bmatrix}. \tag{5}
$$

In addition, there is also a pitching moment $M_{\text{aero},j}$ to be considered, given by

$$M_{\text{aero},j} = \frac{\rho S c}{2}(1-\sigma(\alpha))\left(C_{\text{m}_0} + C_{\text{m}_\alpha}\alpha + C_{\text{m}_\text{e}}\delta_\text{e}\right)\|^{\mathcal{B}}\mathbf{v}\|^2 , \tag{6}$$

with wing mean chord c, pitch coefficient C_{m_0} when $\alpha = 0$ and $\delta_\text{e} = 0$, and pitch static stability coefficient C_{m_α}.

3.2.2 Lateral Aerodynamics

The lateral force component $F_{\text{aero},j}$, the roll $M_{\text{aero},i}$ and the yaw $M_{\text{aero},k}$ components of $\mathbf{F}_\text{aero}$ and $\mathbf{M}_\text{aero}$ are given by

$$F_{\text{aero},j} = \frac{1}{2}\rho S(1-\sigma(\alpha))\left(C_{\text{Y}_\beta}\beta + C_{\text{Y}_\text{a}}\delta_\text{a}\right)\|^{\mathcal{B}}\mathbf{v}\|^2, \tag{7}$$

$$M_{\text{aero},i} = \frac{1}{2}\rho S b(1-\sigma(\alpha))\left(C_{\text{l}_\beta}\beta + C_{\text{l}_\text{a}}\delta_\text{a}\right)\|^{\mathcal{B}}\mathbf{v}\|^2, \tag{8}$$

$$M_{\text{aero},k} = \frac{1}{2}\rho S b(1-\sigma(\alpha))\left(C_{\text{n}_\beta}\beta + C_{\text{n}_\text{a}}\delta_\text{a}\right)\|^{\mathcal{B}}\mathbf{v}\|^2, \tag{9}$$

with sideslip angle β , wingspan b, lateral force coefficient concerning β and δ_a, C_{Y_β} and C_{Y_a}, respectively, roll and yaw static stability coefficients, C_{l_β} and C_{n_β}, deflection control coefficient concerning roll C_{l_a}, and deflection cross-control coefficient concerning yaw C_{n_a}. The aileron deflection angle δ_a is given by $\delta_\text{a} = -\delta_{\text{e,r}} + \delta_{\text{e,l}}$.

3.3. Rotor Forces and Moments

The UAV has two front tilting rotors, one on each wing, and one fixed rotor on its tail. Denoting the right and left rotors by rotor $i = \{1,\ 2\}$, respectively, each spins with angular velocity ω_i, with rotor 1 spinning anticlockwise and rotor 2 clockwise, and generates a force $\mathbf{F}_i$ and a moment $\mathbf{M}_i$, with magnitudes given by $F_i = k_\text{F}\omega_i^2 \frac{1}{2}\rho\, S_\text{rotor}\|\mathbf{v}_{\text{air,rotor}}\|^2$and $M_i = k_\text{M}\omega_i^2$, with k_F and k_M force and moment coefficients related to these rotors, S_rotor the rotor surface area, and $\mathbf{v}_{\text{air,rotor}}$ the velocity of the air going into the rotor. Force $\mathbf{F}_i$ is applied in the direction of $\hat{\boldsymbol{\imath}}_{\mathcal{T}_i}$, and the moment $\mathbf{M}_i$ is applied about the axis $\hat{\boldsymbol{\imath}}_{\mathcal{T}_i}$, with opposite signal relative to the angular velocity ω_i. The overall force $\mathbf{F}_\text{wr}$ and moment $\mathbf{M}_\text{wr}$ from the front rotors acting on the CoM is given by

$$\mathbf{F}_\text{wr} = \begin{bmatrix} F_1\ \cos(\gamma_1) + F_2\ \cos(\gamma_2) \\ 0 \\ -F_1\sin(\gamma_1) - F_2\sin(\gamma_2) \end{bmatrix} \tag{10}$$

$$\mathbf{M}_\text{wr} = \begin{bmatrix} M_1\ \cos(\gamma_1) - M_2\ \cos(\gamma_2) \\ 0 \\ -M_1\sin(\gamma_2) + M_2\sin(\gamma_2) \end{bmatrix} \tag{11}$$

Forces $\mathbf{F}_1$ and $\mathbf{F}_2$ are applied at positions $\mathbf{r}_1$ and $\mathbf{r}_2$, thus generating a moment $\mathbf{M}_{\text{F,wr}}$, given by

$$\mathbf{M}_{\text{F,wr}} = \mathbf{r}_1 \times \left(\tfrac{\mathcal{B}}{\mathcal{T}_1}\mathbf{R}\ \mathbf{F}_1\right) + \mathbf{r}_2 \times \left(\tfrac{\mathcal{B}}{\mathcal{T}_2}\mathbf{R}\ \mathbf{F}_2\right) \tag{12}$$

There is also the force $\mathbf{F}_\text{tr}$ and a moment $\mathbf{M}_\text{tr}$ from the tail rotor, which spins anticlockwise with angular velocity ω_tr, given by $\mathbf{F}_\text{tr} = -F_\text{tr}\,\hat{\boldsymbol{k}}_\mathcal{B}$ and $\mathbf{M}_\text{tr} = M_\text{tr}\,\hat{\boldsymbol{k}}_\mathcal{B}$. The magnitudes are given by $F_\text{tr} = k_{\text{F,tr}}\omega_\text{tr}^2$ and $M_\text{tr} = k_{\text{M,tr}}\omega_\text{tr}^2$, with $k_{\text{F,tr}}$ and $k_{\text{M,tr}}$ the force and moment coefficients for the tail rotor. Since $\mathbf{F}_\text{tr}$ is not applied directly to the CoM, it generates a pitching moment $\mathbf{M}_{\text{F,tr}}$. Consider the position vector $\mathbf{r}_\text{tr}$ with origin in the CoM with magnitude equal to the distance between the CoM and the point where $\mathbf{F}_\text{tr}$ is applied, and pointing to said point. Then, the moment $\mathbf{M}_{\text{F,tr}}$ is $\mathbf{M}_{\text{F,tr}} = \mathbf{r}_\text{tr}\times\mathbf{F}_\text{tr}$, which, assuming that the angle between the position and force vectors $\angle(\mathbf{r}_\text{tr},\ \mathbf{F}_\text{tr}) \approx \frac{\pi}{2}$, then $\mathbf{M}_{\text{F,tr}} = -\|\mathbf{r}_{tr}\|\ k_{\text{F,tr}}\ \omega_\text{tr}^2\ \hat{\boldsymbol{\jmath}}_\mathcal{B}$.

Combining the above expressions, the total force $\mathbf{F}_\text{rotors}$ and moment $\mathbf{M}_\text{rotors}$ generated by the rotors are

$$\begin{aligned} \mathbf{F}_\text{rotors} &= \mathbf{F}_\text{wr} + \mathbf{F}_\text{tr}\,, \\ \mathbf{M}_\text{rotors} &= \mathbf{M}_\text{wr} + \mathbf{M}_\text{tr} + \mathbf{M}_{\text{F,wr}} + \mathbf{M}_{\text{F,tr}}\,. \end{aligned} \tag{13}$$

3.4. Kinematic and Dynamic Equations

Let the position of the CoM w.r.t. $\{\mathcal{I}\}$ be denoted by $\mathbf{p} = \begin{bmatrix} p_x & p_y & p_z \end{bmatrix}^\mathsf{T}$, and the linear velocity of frame $\{\mathcal{B}\}$ relative to $\{\mathcal{I}\}$, expressed in $\{\mathcal{I}\}$, by $\mathbf{v} = \begin{bmatrix} v_x & v_y & v_z \end{bmatrix}^\mathsf{T}$. Further, let $\boldsymbol{q} = (q_0,\, q_1,\, q_2,\, q_3) = (q_0,\, \mathbf{q})$ be the quaternion that represents the UAV's orientation and $\boldsymbol{\omega} = \begin{bmatrix} p & q & r \end{bmatrix}^\mathsf{T}$the UAV's angular velocity. The kinematic equations of motion are

$$\dot{\mathbf{p}} = \mathbf{v}\ , \tag{14}$$

$$\dot{\boldsymbol{q}} = \frac{1}{2}\begin{bmatrix} -q_1 & -q_2 & -q_3 \\ q_0 & q_3 & -q_2 \\ -q_3 & q_0 & q_1 \\ q_2 & -q_1 & q_0 \end{bmatrix}\boldsymbol{\omega}\ . \tag{15}$$

In addition, acting on the UAV are also the force due to gravity $\mathbf{F}_\text{g}$, the aerodynamic forces and moments, $\mathbf{F}_\text{aero}$ and $\mathbf{M}_\text{aero}$, and rotor forces and moments, $\mathbf{F}_\text{rotors}$ and $\mathbf{M}_\text{rotors}$. Hence, the Newton-Euler equations of motion are

$$m\dot{\mathbf{v}} = \mathbf{F}_\text{g} + \tfrac{\mathcal{I}}{\mathcal{B}}\mathbf{R}\,\mathbf{F}_\text{aero} + \tfrac{\mathcal{I}}{\mathcal{B}}\mathbf{R}\,\mathbf{F}_\text{rotors}\ , \tag{16}$$

$$\mathbf{J}\,\dot{\boldsymbol{\omega}} = -\mathbf{S}(\boldsymbol{\omega})\,\mathbf{J}\,\boldsymbol{\omega} + \mathbf{M}_\text{aero} + \mathbf{M}_\text{rotors}\ , \tag{17}$$

with m and $\mathbf{J}$ being the mass and inertia matrix of the UAV, respectively, and $\tfrac{\mathcal{I}}{\mathcal{B}}\mathbf{R}$ the rotation matrix from $\{\mathcal{B}\}$ to the $\{\mathcal{I}\}$. In the absence of wind, the aerodynamic force and moment, as well as the rotors force and moment, may be decomposed into forces and moments that depend solely on the state (more precisely the velocity) of the UAV, $\mathbf{F}_\text{state}(\mathbf{v})$ and $\mathbf{M}_\text{state}(\mathbf{v})$, and on the states and inputs, $\mathbf{F}_\text{inputs}(\mathbf{v},\,\mathbf{u})$ and $\mathbf{M}_\text{inputs}(\mathbf{v},\,\mathbf{u})$, with inputs $\mathbf{u} = \begin{bmatrix} \omega_1 & \omega_2 & \omega_\text{tr} & \gamma_1 & \gamma_2 & \delta_{\text{e,l}} & \delta_{\text{e,r}} \end{bmatrix}$. Thus, (16) and (17) may be rewritten as

$$m\dot{\mathbf{v}} = \mathbf{F}_\text{g} + \tfrac{\mathcal{I}}{\mathcal{B}}\mathbf{R}\left(\mathbf{F}_\text{state} + \mathbf{F}_\text{inputs}\right)\ , \tag{18}$$

$$\mathbf{J}\,\dot{\boldsymbol{\omega}} = -\mathbf{S}(\boldsymbol{\omega})\,\mathbf{J}\,\boldsymbol{\omega} + \mathbf{M}_\text{state} + \mathbf{M}_\text{inputs}\ . \tag{19}$$

This rearrangement will be useful in the control strategy deduced in Section 4.

3.5. Error Dynamics

The system error dynamics will be of importance when deriving the control strategy. To begin, the position error $\widetilde{\mathbf{p}}$ is defined as the difference between the position and its reference and the velocity error $\widetilde{\mathbf{v}}$ as the difference between the velocity and its reference. As such, these two terms are given by

$$\widetilde{\mathbf{p}} = \mathbf{p} - \mathbf{p}_{\text{ref}} \ , \tag{20}$$

$$\widetilde{\mathbf{v}} = \dot{\widetilde{\mathbf{p}}} = \mathbf{v} - \mathbf{v}_{\text{ref}} \ . \tag{21}$$

The time-derivative of the velocity error, the acceleration error $\widetilde{\mathbf{a}}$, is thus given by

$$\dot{\widetilde{\mathbf{v}}} = \widetilde{\mathbf{a}} = \mathbf{g} + \frac{1}{m} {}^{\mathcal{I}}_{\mathcal{B}}\mathbf{R}\, \mathbf{F}_{\text{states}} + \frac{1}{m} {}^{\mathcal{I}}_{\mathcal{B}}\mathbf{R}\, \mathbf{F}_{\text{inputs}} - \mathbf{a}_{\text{ref}} \tag{22}$$

Regarding attitude, the orientation error $\widetilde{\boldsymbol{q}}$, defined as the quaternion product of the orientation reference conjugate by the orientation of the UAV, with a corresponding error rotation matrix $\widetilde{\mathbf{R}}$, and the angular velocity error $\widetilde{\boldsymbol{\omega}}$ are given by

$$\begin{aligned} \widetilde{\boldsymbol{q}} &= (\widetilde{q}_0, \widetilde{\mathbf{q}}) = \bar{\boldsymbol{q}}_{\text{ref}} \circ \boldsymbol{q} \,, \\ \widetilde{\mathbf{R}} &= \mathbf{R}(\widetilde{\boldsymbol{q}}) \,, \\ \widetilde{\boldsymbol{\omega}} &= \boldsymbol{\omega} - \widetilde{\mathbf{R}}\, \boldsymbol{\omega}_{\text{ref}} \,. \end{aligned} \tag{23}$$

The time-derivative of $\widetilde{\boldsymbol{\omega}}$, the angular acceleration error, is given by

$$\begin{aligned} \dot{\widetilde{\boldsymbol{\omega}}} &= \dot{\boldsymbol{\omega}} - \frac{d}{dt}\left(\widetilde{\mathbf{R}}\, \boldsymbol{\omega}_{\text{ref}}\right) \\ &= \mathbf{J}^{-1}\left(-\mathbf{S}(\boldsymbol{\omega})\, \mathbf{J}\, \boldsymbol{\omega} + \mathbf{M}_{\text{states}} + \mathbf{M}_{\text{inputs}}\right) \\ &- \left(\widetilde{\mathbf{R}}\, \dot{\boldsymbol{\omega}}_{\text{ref}} - \mathbf{S}(\widetilde{\boldsymbol{\omega}})\, \widetilde{\mathbf{R}}\, \boldsymbol{\omega}_{\text{ref}}\right) \,. \end{aligned} \tag{24}$$

4. Control

In this section, we describe the control approach and analyse the shortcomings.

4.1. Control System Architecture

The overal control system architecture is shown in Figure 2. The Trajectory Handler provides the trajectory references ($\mathbf{p}_{\text{ref}}$, $\mathbf{v}_{\text{ref}}$, $\mathbf{a}_{\text{ref}}$) to the Controller, which calculates the reference force $\mathbf{F}_{\text{ref}}$ and moment $\mathbf{M}_{\text{ref}}$. The Controller is divided into two blocks: the position controller and attitude controller. The position controller receives the trajectory reference and the UAV state and computes $\mathbf{F}_{\text{ref}}$, the orientation quaternion reference $\boldsymbol{q}_{\text{ref}}$, and the angular velocity reference $\boldsymbol{\omega}_{\text{ref}}$. The attitude controller receives $\boldsymbol{q}_{\text{ref}}$ and $\boldsymbol{\omega}_{\text{ref}}$ and calculates $\mathbf{M}_{\text{ref}}$. The Controller architecture is shown in Figure 3. The Control Allocation block computes the input values $\mathbf{u}$ that generate $\mathbf{F}_{\text{ref}}$ and $\mathbf{M}_{\text{ref}}$, which are then fed into UAV model.

4.2. Position Controller

Regarding the position control, the objective is to have the UAV closely follow the trajectory reference. To drive error dynamics related to linear motion to zero, we first define the system

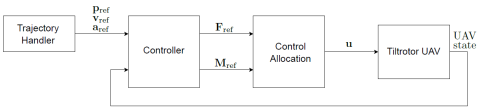

Fig. 2: Control System Architecture

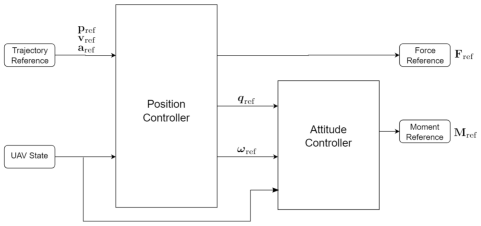

Fig. 3: Controller Architecture

$$\begin{aligned} \boldsymbol{\xi}_1 &= \tilde{\mathbf{p}} \\ \boldsymbol{\xi}_2 &= \tilde{\mathbf{v}} - \boldsymbol{\alpha}_1(\boldsymbol{\xi}_1) \end{aligned} \ , \tag{25}$$

with $\boldsymbol{\alpha}_1(\boldsymbol{\xi}_1)$being the virtual controller to be calculated. A candidate Lyapunov function is proposed, defined as

$$V_1 = \frac{1}{2}\, \boldsymbol{\xi}_1^{\mathsf{T}}\, \boldsymbol{\xi}_1 + \frac{k_{1,\text{I}}}{2} \left[\int \boldsymbol{\xi}_1 dt\right]^{\mathsf{T}} \left[\int \boldsymbol{\xi}_1 dt\right] + \frac{1}{2}\, \boldsymbol{\xi}_2^{\mathsf{T}}\, \boldsymbol{\xi}_2 \,. \tag{26}$$

This Lyapunov function is quadratic in the position error $\boldsymbol{\xi}_1$, in the integral of the position error, and in the velocity error $\boldsymbol{\xi}_2$. Taking the virtual controller to be $\boldsymbol{\alpha}_1(\boldsymbol{\xi}_1) = -k_1\, \boldsymbol{\xi}_1 - k_{1,\text{I}} \left[\int \boldsymbol{\xi}_1 dt\right]$ with constants $k_1 > 0$ and $k_{1,\text{I}} > 0$, it follows that the derivative $\dot{V}_1$ is given by

$$\begin{aligned} \dot{V}_1 = &-k_1\, \|\boldsymbol{\xi}_1\|^2 + \boldsymbol{\xi}_1^{\mathsf{T}}\, \boldsymbol{\xi}_2 + \boldsymbol{\xi}_2^{\mathsf{T}} \left(\mathbf{g} + \frac{1}{m}\mathbf{F}_{\text{state}}\right. \\ &+ \frac{1}{m}\mathbf{F}_{\text{input}} - \mathbf{a}_{\text{ref}} + k_1\, \boldsymbol{\xi}_2 + (k_{1,\text{I}} - k_1^2)\, \boldsymbol{\xi}_1 \\ &\left. -k_1\, k_{1,\text{I}} \left[\int \boldsymbol{\xi}_1 dt\right]\right) \,. \end{aligned} \tag{27}$$

The notation $\mathbf{F}_{\text{state}}$ and $\mathbf{F}_{\text{input}}$ is used, since the goal is to find a force reference that will be generated by the control allocation scheme. Defining $\mathbf{F}_{\text{ref}}$ as the $\mathbf{F}_{\text{input}}$ that stabilises the system, if

$$\begin{aligned} \mathbf{F}_{\text{ref}} = &-\mathbf{F}_{\text{g}} - \mathbf{F}_{\text{state}} + m\,(\, \mathbf{a}_{\text{ref}} - (k_1 + k_2)\, \tilde{\mathbf{v}} \\ &-(1 + k_{1,\text{I}} + k_1 k_2)\, \tilde{\mathbf{p}} - k_{1,\text{I}} k_2 \left[\int \tilde{\mathbf{p}}\, dt\right]\Big) \end{aligned} \ , \tag{28}$$

with $k_2 > 0$, then $\dot{V}_1 = -k_1\, \|\boldsymbol{\xi}_1\|^2 - k_2\, \|\boldsymbol{\xi}_2\|^2 \leq 0$. Thus, with force reference $\mathbf{F}_{\text{ref}}$, the position and velocity errors converge to $\mathbf{0}$.

Calculating the orientation reference for tiltrotor UAVs is not as straightforward as for UAVs with fixed rotors. The approach taken involves an optimisation problem, similar to [6]. The main difficulty stems from the additional degree of freedom

that the tilting rotors provide. The first step is to find an estimate of the tilt angles, fixing the generated force from the front rotors in a certain direction. This does not solve the problem completely, but simplifies it. We assume that the estimated tilt angle is the same for both rotors and that the resulting pitching moment should be zero. The tilt angle estimate γ_{est} is given by

$$\gamma_{\text{est}} = \text{sat}\left(\text{atan2}\left(F_{\text{ref},k}\ ,\ F_{\text{ref},i}\left(1+\frac{r_{1,i}}{r_{\text{tr},i}}\right)\right)\right)\ , \tag{29}$$

which is limited between the maximum and minimum values of the tilt angle. Considering that the rotors tilt in a pitching motion, the current pitch of the UAV influences γ_{est}, but in normal conditions, tiltrotor aircraft are characterised by a small pitch angle in any flight mode.Despite simplifying the attitude reference calculation by setting a tilt angle estimate, it is still complex. To determine the attitude, the problem is formulated as the following optimisation problem:

$$\begin{aligned}
\min_{\phi,\,\theta,\,\psi,F_1,\,F_2,\,F_{\text{tr}}} \quad & \left\|{}^{\mathcal{I}}_{\mathcal{B}}\mathbf{R}(\phi,\,\theta,\,\psi)\ \mathbf{F}_{\text{rotors}} - \mathbf{F}_{\text{ref}}\right\|_2 \\
\text{subject to} \quad & 0 \le F_1\,,\ 0 \le F_2\,,\ 0 \le F_{\text{tr}} \\
& -\tfrac{\pi}{2} \le \phi \le \tfrac{\pi}{2} \\
& \theta_{\min} \le \theta \le \theta_{\max} \\
& -\pi \le \psi \le \pi
\end{aligned} \tag{30}$$

The variables are the roll, pitch and yaw angles, and the forces generated by each rotor, encoded in $\mathbf{F}_{\text{rotors}}$. The objective is to minimise the difference between the reference force and the force generated by rotors in a desired attitude encoded by ${}^{\mathcal{I}}_{\mathcal{B}}\mathbf{R}$. The interference between the aircraft's pitch and tilt angles is addressed by limiting the pitch angle to $[\theta_{\min},\,\theta_{\max}]$. From ${}^{\mathcal{I}}_{\mathcal{B}}\mathbf{R}_{\text{ref}}$, the reference quaternion $\boldsymbol{q}_{\text{ref}}$ can be calculated. Having $\boldsymbol{q}_{\text{ref}}$, the angular velocity reference $\boldsymbol{\omega}_{\text{ref}}$ is proportional to the vector part of the quaternion that results from the multiplication of the $\boldsymbol{q}_{\text{ref}}$ and the current orientation quaternion $\boldsymbol{q}$, i.e. $\boldsymbol{\omega}_{\text{ref}} = k_\omega\ \text{vec}\left(\boldsymbol{q}_{\text{ref}} \circ \boldsymbol{q}\right)$, with $k_\omega > 0$ is a constant and $\text{vec}(\cdot)$ returns the vector part of a quaternion.

4.3. Attitude Controller

Making use of the error dynamics model related to angular motion, we define the system

$$\begin{aligned}
\boldsymbol{\xi}_3 &= \widetilde{\mathbf{q}} \\
\boldsymbol{\xi}_4 &= \widetilde{\boldsymbol{\omega}} - \boldsymbol{\alpha}_2(\boldsymbol{\xi}_3)
\end{aligned}\ , \tag{31}$$

with virtual controller $\boldsymbol{\alpha}_2(\boldsymbol{\xi}_3)$.We propose a candidate Lyapunov function V_2, defined as

$$V_2 = \frac{1}{2}\ \boldsymbol{\xi}_3^{\mathsf{T}}\ \boldsymbol{\xi}_3 + \frac{1}{2}\ \boldsymbol{\xi}_4^{\mathsf{T}}\ \boldsymbol{\xi}_4\,. \tag{32}$$

This Lyapunov function is quadratic in the orientation error $\boldsymbol{\xi}_3$ and the angular velocity error $\boldsymbol{\xi}_4$. Let us denote $\widetilde{\mathbf{Q}} = \left(\mathbf{S}(\boldsymbol{\xi}_3)\ +\ \sqrt{1-\boldsymbol{\xi}_3^{\mathsf{T}}\boldsymbol{\xi}_3}\ \mathbf{I}_{3\times 3}\right)$and define the virtual controller as $\boldsymbol{\alpha}_2(\boldsymbol{\xi}_3) = -2\ k_3\ \widetilde{\mathbf{Q}}^{-1}\ \boldsymbol{\xi}_3$, with constant $k_3 > 0$. Taking the derivative of V_2, we have

$$\begin{aligned}
\dot{V}_2 = &-k_3\ \|\boldsymbol{\xi}_3\|^2 + \frac{1}{2}\ \boldsymbol{\xi}_3^{\mathsf{T}}\ \widetilde{\mathbf{Q}}\ \boldsymbol{\xi}_4 + \\
&\boldsymbol{\xi}_4^{\mathsf{T}}\left(\mathbf{J}^{-1}\left(-\mathbf{S}(\boldsymbol{\omega})\,\mathbf{J}\,\boldsymbol{\omega} + \mathbf{M}_{\text{state}} + \mathbf{M}_{\text{input}}\right)\right. \\
&\left.-\left(\widetilde{\mathbf{R}}\,\dot{\boldsymbol{\omega}}_{\text{ref}} - \mathbf{S}(\widetilde{\boldsymbol{\omega}})\,\widetilde{\mathbf{R}}\,\boldsymbol{\omega}_{\text{ref}}\right) - \dot{\boldsymbol{\alpha}}_2(\boldsymbol{\xi}_3)\right)\ .
\end{aligned} \tag{33}$$

The notation $\mathbf{M}_{\text{state}}$ and $\mathbf{M}_{\text{input}}$ is used as it is more practical to use in the control allocation scheme. Defining $\mathbf{M}_{\text{ref}}$ as the $\mathbf{M}_{\text{input}}$ that accomplishes this, the expression is given by

$$\begin{aligned}
\mathbf{M}_{\text{ref}} = &\ \mathbf{S}(\boldsymbol{\omega})\mathbf{J}\ \boldsymbol{\omega}\ -\ \mathbf{M}_{\text{state}} + \mathbf{J}\left(\widetilde{\mathbf{R}}\ \dot{\boldsymbol{\omega}}_{\text{ref}} - \right. \\
&\left.\mathbf{S}(\boldsymbol{\omega})\ \widetilde{\mathbf{R}}\ \boldsymbol{\omega}_{\text{ref}} + \dot{\boldsymbol{\alpha}}_2(\boldsymbol{\xi}_3) - k_4\ \boldsymbol{\xi}_4 - \frac{1}{2}\ \widetilde{\mathbf{Q}}^{\mathsf{T}}\ \boldsymbol{\xi}_3\right)\ ,
\end{aligned} \tag{34}$$

where $k_4 > 0$ is a constant. With $\mathbf{M}_{\text{ref}}$, $\dot{V}_2 = -k_3\ \|\boldsymbol{\xi}_3\|^2 - k_4\ \|\boldsymbol{\xi}_4\|^2 \le 0$, and the orientation and angular velocity errors converge to $\mathbf{0}$.

4.4. Control Allocation

The control allocation issue is complex, particularly considering a unified control approach. As the system is considered as a whole, depending on the state of the UAV at each instant, the control allocation strategy should be able to calculate the necessary inputs without *a priori* information of the functioning configuration.

The reference trajectories, which will be described in Section 5, deal mostly with longitudinal motion, so longitudinal motion will be given more significance than lateral motion in this allocation scheme. The longitudinal forces and moment depend nonlinearly on $\mathbf{u}_{\text{long}} = \{\omega_1,\,\omega_2,\,\omega_{\text{tr}},\,\gamma_1,\,\gamma_2,\,\delta_{\text{e}}\}$. To allocate these forces and moment, the following optimisation problem is formulated:

$$\begin{aligned}
\underset{\mathbf{u}_{\text{long}}}{\text{minimise}} \quad & \left\|\begin{bmatrix}F_{\text{ref,i}}\\ F_{\text{ref,k}}\\ M_{\text{ref,j}}\end{bmatrix} - \begin{bmatrix}F_{\text{input,i}}(\mathbf{u}_{\text{long}})\\ F_{\text{input,k}}(\mathbf{u}_{\text{long}})\\ M_{\text{input,j}}(\mathbf{u}_{\text{long}})\end{bmatrix}\right\|_2\ , \\
\text{subject to} \quad & \mathbf{u}_{\text{long,min}} \le \mathbf{u}_{\text{long}} \le \mathbf{u}_{\text{long,max}}
\end{aligned} \tag{35}$$

which is solved at each time instant by a nonlinear optimisation solver.

The lateral aerodynamic force and moments depend linearly on δ_{a}. In terms of the rotors, lateral motion can be achieved via differential thrust of the front rotors, depending on the direction given by the tilt angle. Considering the trajectories at hand and to simplify the problem, an equal tilt angle γ is assumed, given by the average of the angles calculated in (35), making the lateral moments related to the rotors dependent on $\omega_{\text{d}} = (\omega_1^2 - \omega_2^2)$. The allocation problem is formulated as the following constrained

least squares problem

$$\underset{\omega_{\mathrm{d}},\delta_{\mathrm{a}}}{\text{minimise}} \left\| \begin{bmatrix} c_{11} & c_{12} \\ c_{21} & c_{22} \\ c_{31} & c_{32} \end{bmatrix} \begin{bmatrix} \omega_{\mathrm{d}} \\ \delta_{\mathrm{a}} \end{bmatrix} - \begin{bmatrix} F_{\mathrm{ref,j}} \\ M_{\mathrm{ref,i}} \\ M_{\mathrm{ref,k}} \end{bmatrix} \right\|_2^2$$

subject to

$$\begin{aligned} &\delta_{\mathrm{a,min}} \leq \delta_{\mathrm{a}} \leq \delta_{\mathrm{a,max}} \\ &c_{11} = 0\,, && c_{12} = 0.5\rho S(1-\sigma(\alpha))C_{\mathrm{Y_a}} \\ &c_{21} = -r_{1,\mathrm{y}} k_{\mathrm{F}} \sin(\gamma)\,, && c_{22} = 0.5\rho S b(1-\sigma(\alpha))C_{\mathrm{l_a}} \\ &c_{31} = -r_{1,\mathrm{y}} k_{\mathrm{F}} \cos(\gamma)\,, && c_{32} = 0.5\rho S b(1-\sigma(\alpha))C_{\mathrm{n_a}} \end{aligned} \tag{36}$$

This control allocation approach presents limitations that are addressed next.

4.5. Limitations

Concerning the attitude reference, the pitch angle influences γ_{est}, which is addressed by assuming that the pitch angle is always constrained between θ_{min} and θ_{max}. This may not hold at all times and could jeopardise the computation of the orientation reference. Formulating the attitude reference generation and the control allocation as a nonlinear optimisation problems creates further issues. The solver may take excessive time to solve the problem or fail to find a solution, which is not viable for a real world application, and results may vary depending on the solver used. In the control allocation, the division into longitudinal and lateral dynamics, made to reduce the complexity, gives more significance to the longitudinal dynamics, at the expense of the lateral dynamics. An approach that takes into account both simultaneously and has a closed-form solution would be preferable, though such is difficult to obtain without some trade-off.

5. Simulation

In this section, the simulation results are presented for two trajectories that are introduced next. The UAV is set to initially be at rest, in the origin of the inertial frame, and with its body frame aligned with the inertial frame. The simulations were performed using Matlab and Simulink.

The reference trajectories are simply the concatenation of a vertical and a horizontal segment. Figures 4, 5, and 6 show the position, velocity, and acceleration profiles, respectively, in the $\hat{\boldsymbol{\imath}}_{\mathcal{I}}$, $\hat{\boldsymbol{\jmath}}_{\mathcal{I}}$, and $\hat{\boldsymbol{k}}_{\mathcal{I}}$ axes, of two trajectories denoted by Trajectory A and Trajectory B. In Trajectory A, the forward velocity is the UAV's trim velocity, and in Trajectory B, the forward velocity is lower than trim. Both trajectories share the same upward segment, which presents a trapezoidal velocity profile. The initial position is $\mathbf{p}_{\mathrm{i}} = \begin{bmatrix} 0 & 0 & 0 \end{bmatrix}$ and the final position is $\mathbf{p}_{\mathrm{h}} = \begin{bmatrix} 0 & 0 & -2 \end{bmatrix}$ m, i.e at an altitude of 2 m. In the forward segment, the UAV should accelerate at $a_{\mathrm{for}} = 7.5\,\mathrm{m/s^2}$ for both trajectories. For Trajectory A, the forward velocity is $v_{\mathrm{for}} = 35.75\,\mathrm{m/s}$, and, for Trajectory B, $v_{\mathrm{for}} = 25\,\mathrm{m/s}$. The trim

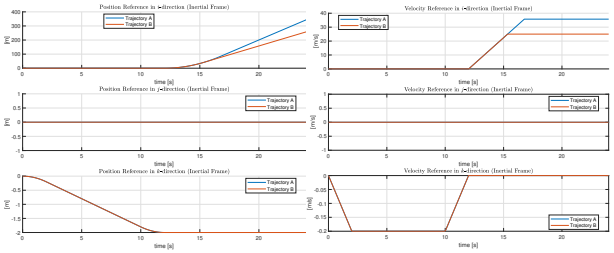

Fig. 4: Position Reference

Fig. 5: Velocity Reference

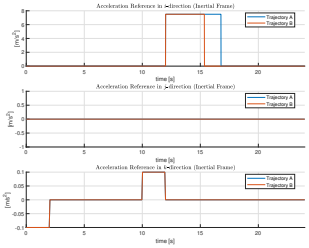

Fig. 6: Acceleration Reference

velocity value was calculated assuming an angle of attack of zero degrees. The reference acceleration values were tuned in simulation. The upward segment takes place in $t = [0, 12]\,\mathrm{s}$, followed by the forward segment from then on. The plots are truncated at $t = 24\,\mathrm{s}$.

Figures 7 and 8 show the plots of the reference and actual position for Traj. A and B, respectively. In both cases, he UAV follows the reference, climbing to an altitude of 2 m in the first 12 s and moving forward from then on at the same altitude. The UAV also adequately tracks the velocity reference, Figures 9 and 10, especially in the $\hat{\boldsymbol{\imath}}_{\mathcal{I}}$ and $\hat{\boldsymbol{\jmath}}_{\mathcal{I}}$ axes, keeping its velocity at zero in both directions during the upward segment, and then following the forward velocity reference during the forward flight segment. In both cases, the velocity reference tracking in the $\hat{\boldsymbol{k}}_{\mathcal{I}}$ axis presents a small error when the UAV begins moving forward, gaining downward velocity, but corrects it and stays levelled.

Figures 11 and 12 show the orientation results, described in Euler angles for a more intuitive analysis, and Figures 13 and 14 show the angular velocity results. One concludes that the attitude reference only acts on the longitudinal dynamics, which is reasonable since only forward motion is required. It is also noticeable that the UAV is not always able to follow the orientation and angular velocity references, particularly at the beginning and end of the forward acceleration part of the trajectory, when the orientation reference presents some brief spikes to negative pitch values on an otherwise constant reference of zero pitch angle. A difference in the forward flight is clear, with the Traj. A results being smoother, whereas the Traj. B results present

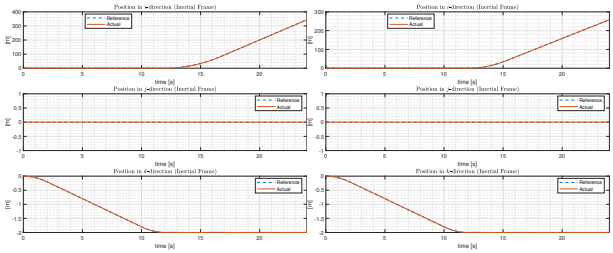

Fig. 7: Traj. A: Position

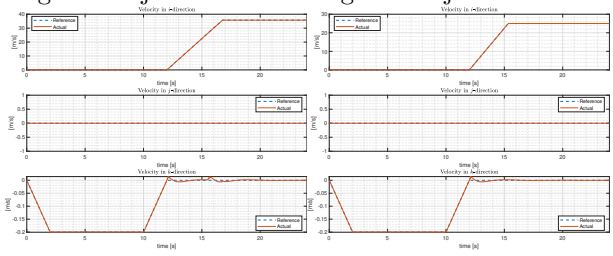

Fig. 8: Traj. B: Position

Fig. 9: Traj. A: Velocity

Fig. 10: Traj. B: Velocity

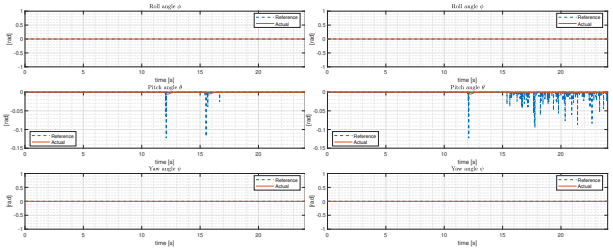

Fig. 11: Traj. A: Orientation

Fig. 12: Traj. B: Orientation

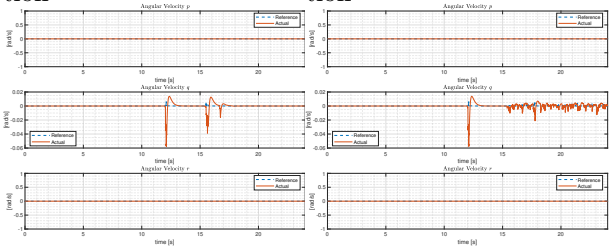

Fig. 13: Traj. A: Angular velocity

Fig. 14: Traj. B: Angular velocity

more irregularities. Despite these irregularities, the pitch angle remains close to zero throughout both trajectories. The pitching angular velocity q follows the reference after the spikes that result from the beginning and end of the forward acceleration, in Traj. A, and presents oscillatory behaviour around the reference, in Traj. B.

The forces and moments allocated by the control allocation scheme and generated by the actuators, w.r.t. $\{\mathcal{B}\}$, for both trajectories are shown in Figures 15 to 18. Considering first the force, during the upwards segment which is equal for Traj. A and B, the reference in the $\hat{\boldsymbol{\imath}}_{\mathcal{B}}$ and $\hat{\boldsymbol{\jmath}}_{\mathcal{B}}$ axes is zero, and in the $\hat{\boldsymbol{k}}_{\mathcal{B}}$ axis opposes the force of gravity. As the UAV starts moving forward, there is a sharp increase in the forward force reference as soon as it begins accelerating. The reference force keeps increasing up until the point when the UAV stops accelerating. The reference in the $\hat{\boldsymbol{k}}_{\mathcal{B}}$ axis decreases in magnitude as the UAV moves forward, as more lift is provided by the wings. In the final part of Traj. A, the forward force is $\approx 39.8\,\text{N}$ and the vertical force is $-7.5\,\text{N}$. In the corresponding part of Traj. B, the forward force is $\approx 23.3\,\text{N}$ and the vertical force is $-70.4\,\text{N}$, but present small magnitude irregularities. The force reference in the $\hat{\boldsymbol{\jmath}}_{\mathcal{B}}$ axis is zero throughout both trajectories. Examining the moments, during the upward motion, the required moments in all body axes are zero, as the UAV's attitude should remain constant. Since the attitude only changes in terms of the pitch angle, it is natural that only the pitching moment reference changes and the other two remain zero. For Traj. A, in forward flight, the pitching moment reference stabilises at $\approx 2\,\text{Nm}$ and during the acceleration part it presents two brief spikes of $\approx -5\,\text{Nm}$, caused by starting and stopping accelerating and by the reduction of the tail rotor angular velocity at $t = 15.5\,\text{s}$. For Traj. B, the pitching moment exhibits irregular behaviour, contrasting with the results of the UAV in trim flight. Nonetheless, from the plots, one concludes that the control allocation scheme is able to allocate the references through the trajectory.

Considering the rotors' angular velocities as well as the tilt and elevon angles, throughout both trajectories, presented in Figures 19 to 22, once more the behaviour during first segment of each trajectory is the same, with elevons fixed at zero deflection and rotors tilted upwards. As the UAV accelerates forward, the front rotors tilt forward and spin faster, the tail rotor initially speeds up to compensate the pitching moment but then begins spinning slower, and the elevons deflect upwards. For Traj. A, in constant velocity forward flight, the front rotors are fully tilted forward and spinning at $13.6\,\text{rad/s}$, the tail rotor stops working, and the elevons stabilise at $-0.02\,\text{rad}$. For Traj. B, the front rotors are tilted at $\approx 28.6°$ (with some brief small magnitude spikes) and spinning at $8.8\,\text{rad}$, the tail rotor at $4.6\,\text{rad/s}$ with some irregularities, and the elevons deflected at $\approx -0.2\,\text{rad}$ also with short small magnitude spikes.

Taking everything into account, the UAV is able to follow the trajectories, keeping a levelled attitude throughout, and the required forces and moments are allocated. Furthermore, in the forward flight part of Traj. A, the tail rotor stops and the front rotors are fully tilted forwards, meaning that the UAV is functioning as a fixed-wing aircraft, and in Traj. B, the UAV stays in an intermediate state,

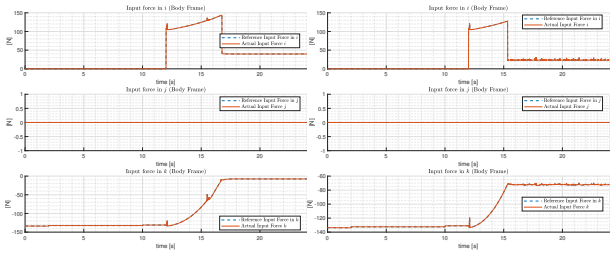

Fig. 15: Traj. A: Force in body

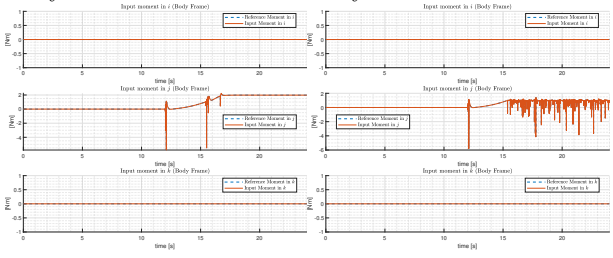

Fig. 16: Traj. B: Force in body

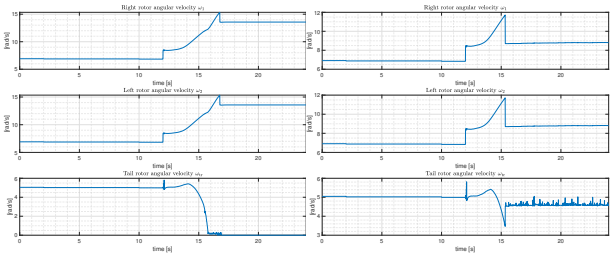

Fig. 19: Traj. A: Rotors' angular velocities

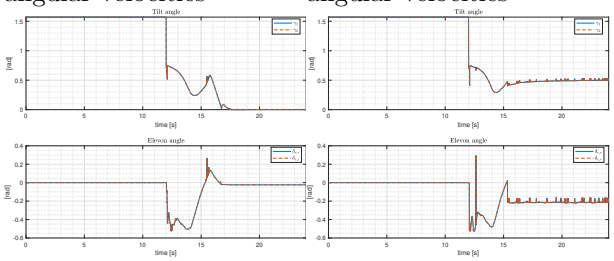

Fig. 20: Traj. B: Rotors' angular velocities

Fig. 17: Traj. A: Moment in body

Fig. 18: Traj. B: Moment in body

Fig. 21: Traj. A: Tilt and Elevon angles

Fig. 22: Traj. B: Tilt and Elevon angles

with the front rotors tilted at a certain angle and the tail rotor still providing lift.

6. UAV Instrumentation

The objective is to equip an *E-Flite Convergence VTOL* with a PX4-compatible autopilot that will allow to control the UAV via remote control and with a ground station, to perform real flight tests, as well as to implement and test different control algorithms. Due to the size of the vehicle and the space available, the chosen autopilot is a Pixhawk 4 Mini. Communication with the autopilot is done via radio and WiFi, so the vehicle was equipped with a FrSky RX8R radio receiver which connects to the RC IN port to fly the UAV in RC mode, and with an ESP8266 WiFi module which connects to the TELEM1 port to communicate with a ground control station. The *E-Flite Convergence VTOL* has three rotors with brushless motors, which are controlled by PWM signals, and connect to ports MAIN 1 to 3 of the autopilot. To supply power, the motors' power connections are soldered directly to the power module board. The tilt and elevon angles are controlled by servo motors. The right and left tilt servo motors connect to MAIN 5 and 6, and the right and left elevon servo motors to MAIN 7 and 8. To connect the servo motors to these ports, a BEC also has to be connected to MAIN 8. Power is supllied by a 3-cell Li-Po 11.1 V, 2600 mAh battery, which fits on the top of the UAV. Reflective markers were also mounted on the UAV for usage with a motion capture system. All these components were assembled on the *E-Flite Convergence VTOL*. Figure 23 shows the top and bottom view of the UAV,

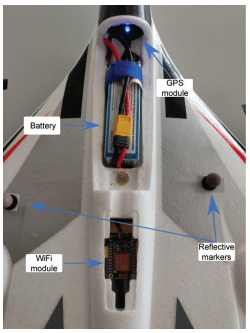

(a) Top view

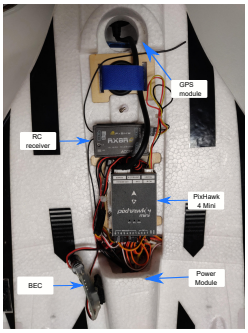

(b) Bottom view

Fig. 23: Assembled components on the *E-flite Convergence VTOL*

displaying the arrangement of all parts.

To validate the instrumentation, a short test flight was conducted, with the UAV controlled via RC, connected via WiFi to a computer running ground control software and with a motion capture system acquiring position data. A video of this test flight can be viewed at https://youtu.be/iLmCVTZQYOs.

7. Conclusions and Future Work

The main objective of this work was to take the first steps in developing a unified control approach that could be used by tri-tilrotor UAVs for trajectory tracking. First, a model of a tri-tilrotor was derived. Afterwards, the control system architecture was presented, with the description of the inner attitude control loop and an outer position control loop, which generated force and moment references

via backstepping. These controllers guaranteed stability, provided that the force and moment references were correctly allocated. Hence, a control allocation scheme was proposed next, which gave more importance to force and moment references related to longitudinal motion, due to the trajectories that would be considered. These strategies presented some limitations, e.g. the time taken by the optimisation solvers to compute the solution, which were discussed. Then, two trajectories of interest were defined. The trajectories differed in the velocity of the forward motion segment, with the desired velocity in the first trajectory being the UAV's trim velocity, and lower in the second trajectory, in order to observe if in the former the UAV would fully transition into a fixed-wing configuration and if in the latter it would fly in an intermediate configuration. To validate the proposed unified control approach, simulations were performed for the two trajectories. The UAV was able to follow the references and executed them in the anticipated configurations. However, in the second trajectory, certain references, as well as the inputs, presented an irregular behaviour when compared to the first case. Finally, the *E-Flite Convergence VTOL*, was equipped with the Pixhawk 4 Mini autopilot to be able to perform real flight tests. To verify the assembly was correct, a test flight was performed.

In terms of future work, it would be advantageous to have better knowledge of the aerodynamic coefficients and other parameter values for the *E-Flite Convergence VTOL*, which could be obtained via fluid dynamics simulations or wind tunnel testing, so as to perform more accurate simulations and improve the controller performance. The matter of the transition from forward flight to hover is also worth researching, in order to complete the range of possible manoeuvres. Another issue that requires further work is the computation of the orientation and angular velocity references and the control allocation, which are done by solving a nonlinear optimisation problem. Moreover, for the control allocation problem, the longitudinal and lateral dynamics were considered disproportionately, which was reasonable for the trajectories considered, but would not be for every trajectory. Research into this matter to find a better approach, possibly one with a closed-form solution, is necessary. Finally, mounting a companion computer on the UAV to implement and test the control approach described in this dissertation, or an improved version, is a significant line of work to follow as well.

References

[1] B. J. Guerreiro, "REPLACE Project." [Online]. Available: http://replace.isr.tecnico.ulisboa.pt

[2] D. A. Ta, I. Fantoni, and R. Lozano, "Modeling and control of a tilt tri-rotor airplane," in *Proceedings of the American Control Conference*, 2012, pp. 131–136.

[3] L. Yu, D. Zhang, J. Zhang, and C. Pan, "Modeling and attitude control of a tilt tri-rotor UAV," in *Chinese Control Conference, CCC*. IEEE Computer Society, 9 2017, pp. 1103–1108.

[4] B. Yuksek, A. Vuruskan, U. Ozdemir, M. A. Yukselen, and G. Inalhan, "Transition Flight Modeling of a Fixed-Wing VTOL UAV," *Journal of Intelligent and Robotic Systems: Theory and Applications*, vol. 84, no. 1-4, pp. 83–105, 2016.

[5] P. Hartmann, C. Meyer, and D. Moormann, "Unified velocity control and flight state transition of unmanned tilt-wing aircraft," *Journal of Guidance, Control, and Dynamics*, vol. 40, no. 6, pp. 1348–1359, 2017.

[6] J. Zhou, X. Lyu, Z. Li, S. Shen, and F. Zhang, "A unified control method for quadrotor tail-sitter UAVs in all flight modes: Hover, transition, and level flight," in *IEEE International Conference on Intelligent Robots and Systems*, vol. 2017-Septe. Institute of Electrical and Electronics Engineers Inc., 12 2017, pp. 4835–4841.

[7] "Control Allocation: reworking the PX4 mixing system — PX4 Developer Summit Virtual 2020." [Online]. Available: https://youtu.be/xjLM9whwjO4

[8] R. W. Beard and T. W. McLain, *Small unmanned aircraft: Theory and practice*. Princeton University Press, 2012.

[9] F. Kendoul, I. Fantoni, and R. Lozano, "Modeling and control of a small autonomous aircraft having two tilting rotors," in *Proceedings of the 44th IEEE Conference on Decision and Control, and the European Control Conference, CDC-ECC '05*, vol. 2005, 2005, pp. 8144–8149.